



Figures and figure supplements

Lunatic fringe-mediated Notch signaling regulates adult hippocampal neural stem cell maintenance

Fatih Semerci et al

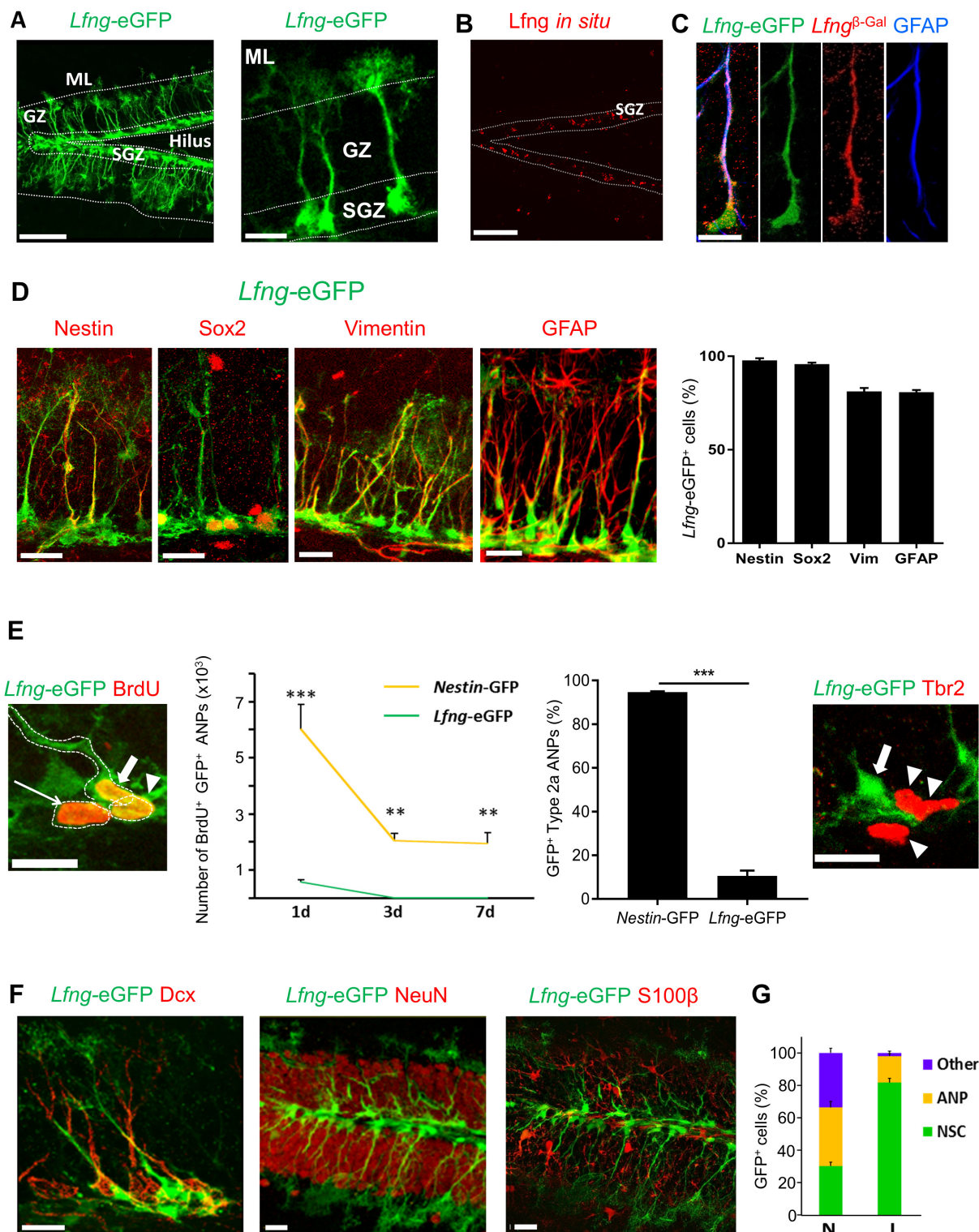


Figure 1. *Lfng-eGFP* is expressed in the NSCs of dentate gyrus. (A) Left panel: Confocal photomicrograph of the dentate gyrus in 2 month-old *Lfng-eGFP* mouse shows *Lfng-eGFP* expressing cells in the subgranular zone only. Right panel: *Lfng-eGFP* expressing cells have typical NSC morphology: Figure 1 continued on next page

Figure 1 continued

triangular cell body in the subgranular zone, a single radial process spanning the granular zone, and fine terminal arborizations in the molecular layer. ML=molecular layer, GZ=granule cell zone, SGZ=subgranular zone. (B) In situ hybridization against the *Lfng* mRNA shows probe expression in the SGZ. Dotted lines indicate the borders of SGZ. (C) In a double transgenic *Lfng*^{Tm1Grid};*Lfng*-eGFP mouse, β -galactosidase (β -Gal) and eGFP are co-expressed, confirming that *Lfng* promoter guiding the eGFP expression is active in the same cells that express β -Gal. *Lfng*^{Tm1Grid}=*Lfng* ^{β -Gal} mouse that carries β -Gal insertion in the *Lfng* locus. (D) *Lfng*-eGFP colocalizes with other NSC markers, such as Nestin, Sox2, Vimentin, and GFAP. Confocal photomicrographs of the representative examples and relative quantitation is shown. (E) eGFP is briefly retained in the first progeny of NSC. *Left panel*: *Lfng*-eGFP expressing cell (thick arrow) and its immediate ANP progeny (arrowhead) are both BrdU⁺ and in cytoplasmic contact. BrdU⁺ ANP not in the cytoplasmic contact with the BrdU⁺ NSC has very low eGFP expression (thin arrow). *Left graph*: eGFP is cleared from BrdU⁺ ANPs between 1 to 3 days following a single dose of BrdU, corresponding to the half-life of GFP protein (N = 3–5 per group, p<0.001 or p<0.0001 for pairwise comparisons of all timepoints, ANOVA with Tukey post-hoc test). *Right graph*: *Lfng*-eGFP is expressed only in minority of Type2a ANPs (Sox2⁺ GFAP⁺ cells in the SGZ; 10.58 \pm 2.38, N = 3), unlike *Nestin*-GFP (94.7 \pm 0.34, N = 4). *Right panel*: Late, Tbr2⁺ ANPs (arrowheads) do not express *Lfng*-eGFP. Arrow points to *Lfng*-eGFP NSC. (F) *Lfng*-eGFP does not co-localize with the markers of neuronal lineage (Dcx⁺ neuroblasts and immature neurons, and NeuN⁺ granule cells) nor S100 β ⁺ astrocytes. (G) While in the *Nestin*-GFP (N) mice GFP is expressed in NSCs, ANPs, and other cell types throughout the dentate gyrus in approximately equal proportions (30.16 \pm 2.43 NSCs, 36.12 \pm 3.73 ANPs, 33.71 \pm 2.81 other cell types), in the *Lfng*-eGFP (L) mice it is expressed predominantly in NSCs (81.68 \pm 2.62% NSCs, 16.37 \pm 1.54% ANPs, 1.95 \pm 1.14% other cell types; N = 4 per genotype). Bars represent mean \pm SEM. **p<0.001, ***p<0.0001. Scale bars = 100 μ m (A left, (B)), 20 μ m (A right, (C–F)). See **Figure 1—figure supplement 1** for further details.

DOI: 10.7554/eLife.24660.002

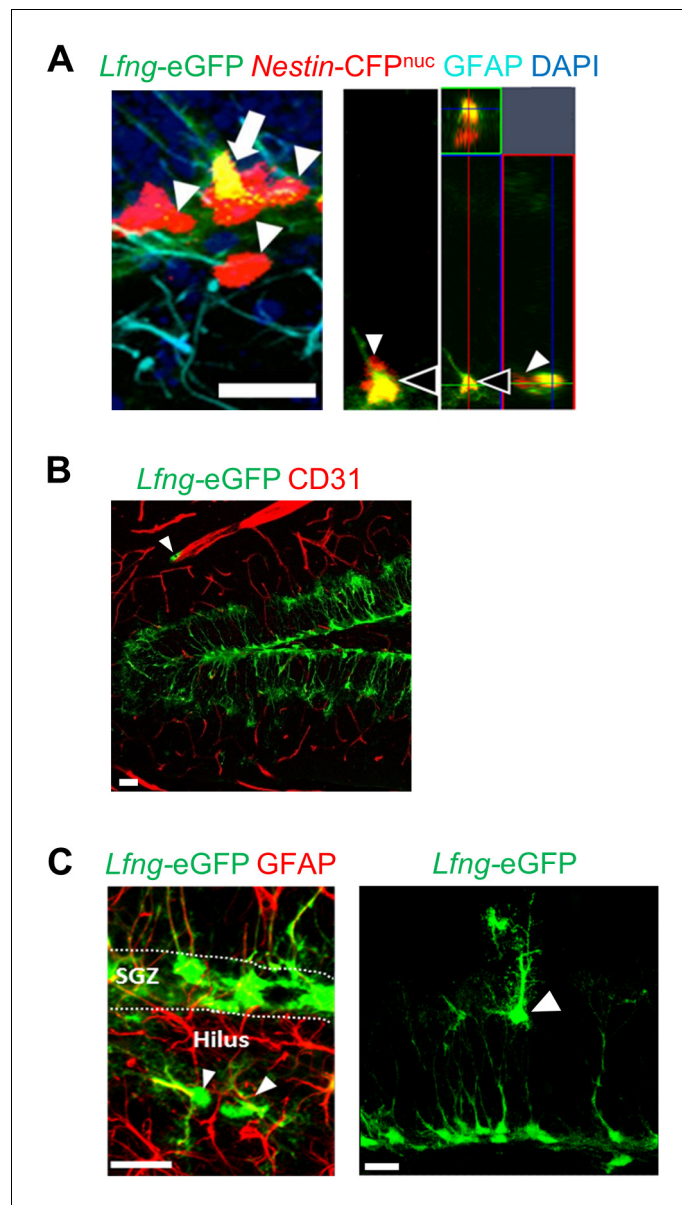


Figure 1—figure supplement 1. *Lfng*-eGFP labels a small number of non-NSC cell types in the dentate gyrus. (A) In a double transgenic *Lfng*-eGFP; *Nestin*-CFP^{nuc} mouse, NSCs express both CFP and eGFP, and have a radial GFAP⁺ process (arrow). Those that express only CFP have round morphology with no processes and are presumed ANPs (arrowheads). Orthogonal projection shows a NSC expressing both *Lfng*-eGFP and *Nestin*-CFP^{nuc} (black arrowhead) and a neighboring ANP expressing only *Nestin*-CFP^{nuc} (white arrowhead). Scale bar = 20 μm. (B) *Lfng*-eGFP is expressed in tip-like cells in close proximity to the endothelial cells immunolabeled with CD31 (arrowhead). Scale bar = 20 μm. (C) Random unidentified *Lfng*-eGFP⁺ cells are detected in the hilus (left panel; arrowhead) and molecular layer (right panel; arrowhead). Scale bar = 20 μm.

DOI: [10.7554/eLife.24660.003](https://doi.org/10.7554/eLife.24660.003)

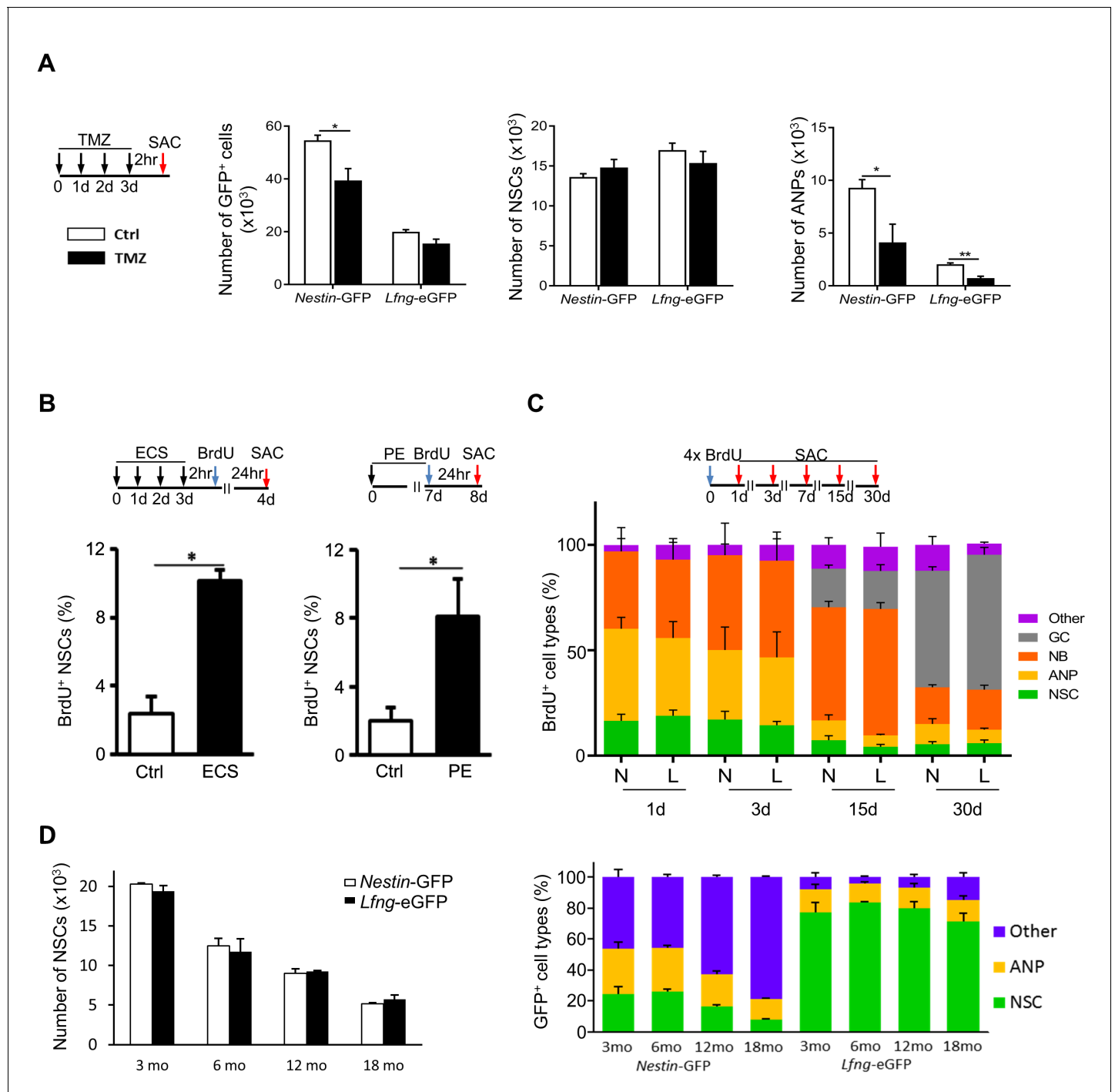


Figure 2. *Lfng*-eGFP-expressing cells are functional NSCs. (A) Most *Lfng*-eGFP⁺ NSCs are quiescent. Bar graphs represent the total number of GFP⁺ cells (left panel), GFP⁺ NSCs (middle panel) and GFP⁺ ANPs (right panel) in 3 month-old *Nestin*-GFP and *Lfng*-eGFP mice (N = 4 per genotype) treated with temozolomide (TMZ). The difference between the two mouse models is most notable with respect to ANPs: while *Nestin*-GFP labels a large number of ANPs, *Lfng*-eGFP does not - it labels primarily quiescent cells. (B) Electroconvulsive shock (ECS) and physical exercise (PE) both activate *Lfng*-eGFP⁺ NSCs (N = 4 per group in ECS and N = 6 per group in PE). (C) *Lfng*-eGFP NSCs produce neuronal progeny. The relative number of newborn, BrdU⁺ progeny was quantified over a 30 day period (NSCs: *Nestin*-GFP⁺ or *Lfng*-eGFP⁺ cells with GFAP⁺ radial processes; ANPs: GFAP⁺ Dcx⁺ NeuN⁺; NBs: Dcx⁺ neuroblasts and immature neurons; GCs: NeuN⁺; Other: BrdU⁺ Dcx⁺ NeuN⁺ cells outside the SGZ; N = 4 per genotype per timepoint). Cumulative BrdU paradigm (four 150 mg/kg injections given 2 hr apart) was used to increase the yield of labeled newborn cells. N=*Nestin*-GFP mice, L=*Lfng*-eGFP mice. (D) The number of *Lfng*-eGFP⁺ NSCs declines over an 18 month period comparably to the number of *Nestin*-GFP⁺ NSCs (left panel; N = 4 per timepoint per genotype). However, the contribution of GFP⁺ cell types in the *Nestin*-GFP and *Lfng*-eGFP mice differs at different

Figure 2 continued on next page

Figure 2 continued

age (right panel). While *Lfng*-eGFP remains selective for NSCs during aging ($p > 0.15$ for all timepoints, Tukey post-hoc test), *Nestin*-GFP labels significantly more non-neuroprogenitors in older mice ($p < 0.002$; Tukey post-hoc test). Bars represent mean \pm SEM. NS=non-significant, * $p < 0.05$, ** $p < 0.001$. See **Figure 2—figure supplement 1** for further details.

DOI: [10.7554/eLife.24660.004](https://doi.org/10.7554/eLife.24660.004)

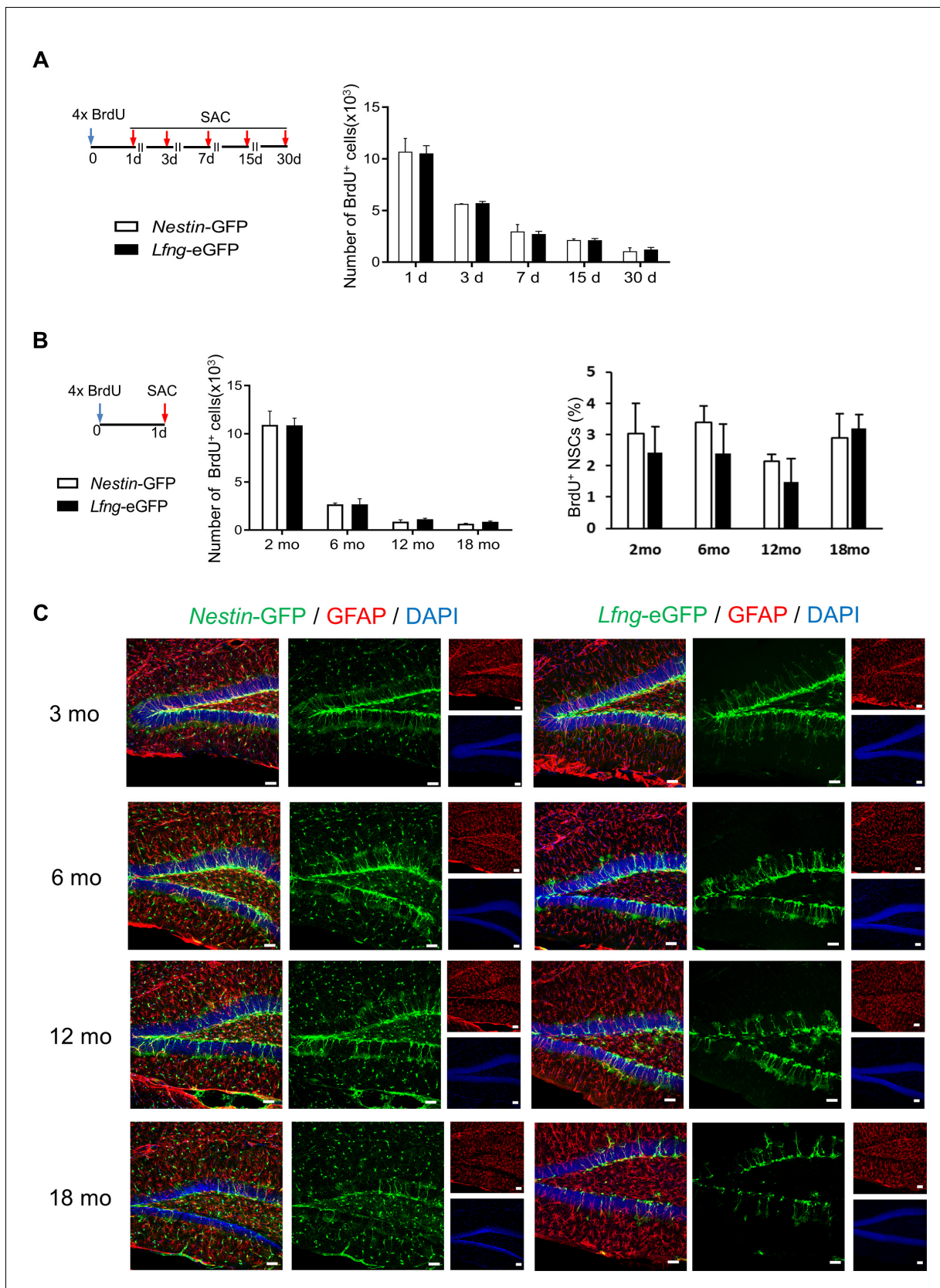


Figure 2—figure supplement 1. The specificity of *Lfng*-eGFP expression for NSCs does not change over time. (A) The total number of BrdU⁺ cells (NSCs and their progeny) in *Nestin*-GFP and *Lfng*-eGFP mice over a 30 day period indicates that cell survival is similar in both mouse models. (B) Figure 2—figure supplement 1 continued on next page

Figure 2—figure supplement 1 continued

Neither the total number BrdU⁺ cells (*left panel*) nor the relative number of BrdU⁺ NSCs (*right panel*) in *Nestin*-GFP and *Lfng*-eGFP mice significantly differs over the 18 month period investigated (N = 4 per genotype per timepoint), indicating that the proliferative capacity of NSCs in the two mouse models is similar. (C) Confocal photomicrographs are representative examples of the dentate gyri of *Nestin*-GFP and *Lfng*-eGFP mice at a given age. Note a decline in the number of GFP⁺ NSCs in both models. However, while the GFP⁺ non-progenitors ('other cells') prevail as the *Nestin*-GFP mice age, in the *Lfng*-eGFP mice eGFP remains expressed in NSCs and the contribution of the GFP⁺'other cells' is minimal. See **Figure 2D** for quantification. Bars represent mean \pm SEM. Scale bar = 20 μ m.

DOI: [10.7554/eLife.24660.005](https://doi.org/10.7554/eLife.24660.005)

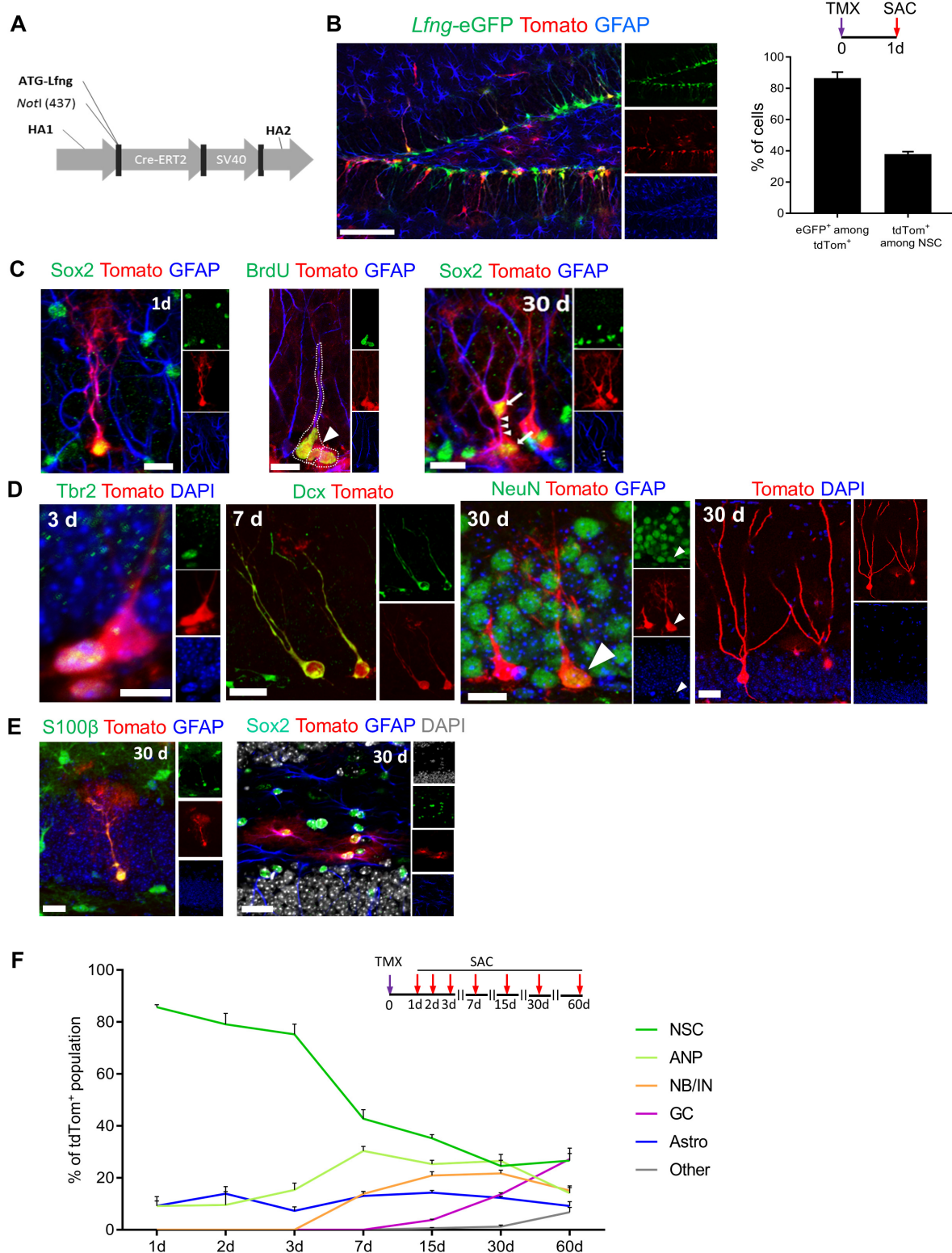


Figure 3. *Lfng*-expressing NSCs generate diverse progeny. (A) The map of bacterial artificial chromosome (BAC) construct used to generate the *Lfng*-CreER^{T2} mouse. (B) In *Lfng*-CreER^{T2}; RCL-tdT; *Lfng*-eGFP triple transgenic mouse, tdTomato⁺ and eGFP⁺ co-expressing cells demonstrate the

Figure 3 continued on next page

Figure 3 continued

specificity of the *Lfng*-CreER^{T2} line to NSCs. *Left panel*: Confocal photomicrograph of the dentate gyrus of a 6 month-old mouse shows the overlapping expression of eGFP and CreER^{T2}-controlled tdTomato one day following tamoxifen injection (TMX; 120 mg/kg). *Right panel*: Quantification of the co-expression of tdTomato⁺ and eGFP⁺ in induced *Lfng*-CreER^{T2}; RCL-tdT mice (N = 3). Bars represent mean±SEM. (C) TMX-induced cells have NSC morphology and divide both asymmetrically and symmetrically. *Left panel*: tdTomato⁺ NSC co-expresses GFAP and Sox2. *Middle panel*: tdTomato⁺ NSC (arrow) divides asymmetrically to produce ANP (arrowhead). *Right panel*: NSC divides symmetrically to produce two cells (arrows) with prominent GFAP⁺ radial processes. *Scale bars* = 20 μm. (D) tdTomato⁺ NSCs produce new neurons through established cascade of cell types, from Tbr2⁺ late ANPs (Type 2b cells), through Dcx⁺ immature neurons, to NeuN⁺ granule cells. *Scale bars* = 20 μm. (E) tdTomato⁺ NSCs also produce S100β astrocytes (or astrocyte-like cells) within the granule cell layer (*left panel*), as well as stellar Sox2⁺ GFAP⁺ cells in the hilus (*right panel*) *Scale bars* = 20 μm. (F) Fate mapping of tdTomato⁺ cells following TMX induction in *Lfng*-CreER^{T2}; RCL-tdT mice reveals that NSCs form the majority (85.7% ± 0.9) of the induced cells at 1dpi, but progressively decline in ratio as they give rise to different progeny over the course of 2 months (N = 3–5 per timepoint). See

Figure 3—figure supplement 1 for further details.

DOI: [10.7554/eLife.24660.006](https://doi.org/10.7554/eLife.24660.006)

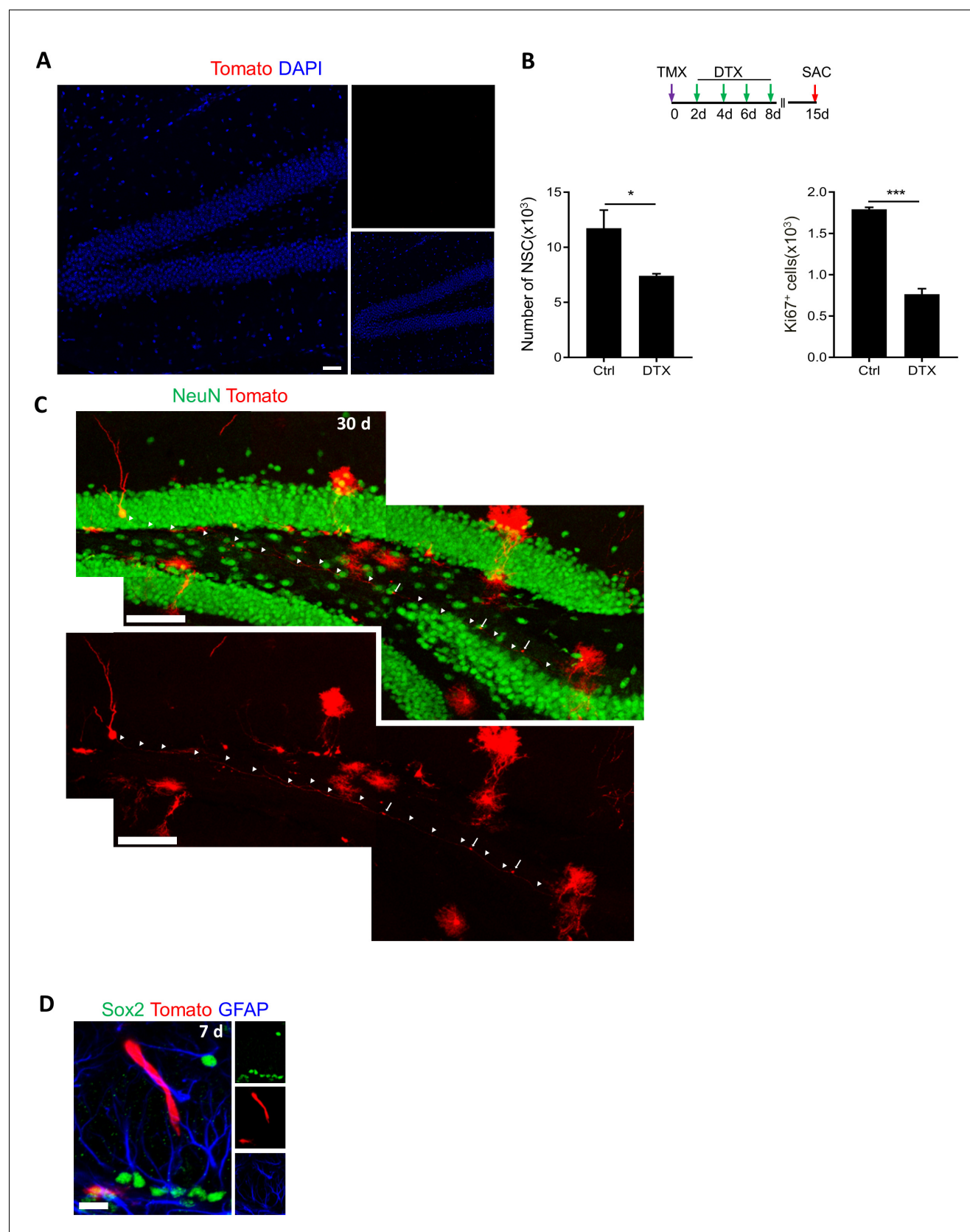


Figure 3—figure supplement 1. *Lfng-CreERT²* expressing cells are NSCs giving rise to newborn neurons. (A) tdTomato expression in *Lfng-CreERT²*; RCL-tdT animals 3 months following vehicle treatment. No tdTomato is observed, indicating no leakage. Scale bar = 50 μ m. (B) Both the number of Figure 3—figure supplement 1 continued on next page

Figure 3—figure supplement 1 continued

NSCs ($N = 4$, $p=0.039$) and the number of cycling $Ki67^+$ cells ($N = 4$, $p<0.0001$) significantly decline following diphtheria toxin (DTX) injection in *Lfng-CreER^{T2}; iDTR* mice, further confirming the stemness of *Lfng*-expressing NSCs. DTR expression in *Lfng-CreER^{T2}; iDTR* mice was induced by tamoxifen (TMX (day 0), followed by four injections of DTX (16 $\mu\text{g/kg}$) two days apart to kill *Lfng-CreER^{T2}* derivatives. Mice were sacrificed at 15 days post-induction. (C) A confocal photomicrograph of a newborn neuron with prominent dendritic spines and axonal projections to CA3 region, observed at 30 days post-induction in *Lfng-CreER^{T2}; RCL-tdT*. Scale bar = 100 μm . (D) Occasionally, tdTomato⁺ tip cells were observed following induction in *Lfng-CreER^{T2}; RCL-tdT* mice. Scale bar = 20 μm .

DOI: [10.7554/eLife.24660.007](https://doi.org/10.7554/eLife.24660.007)

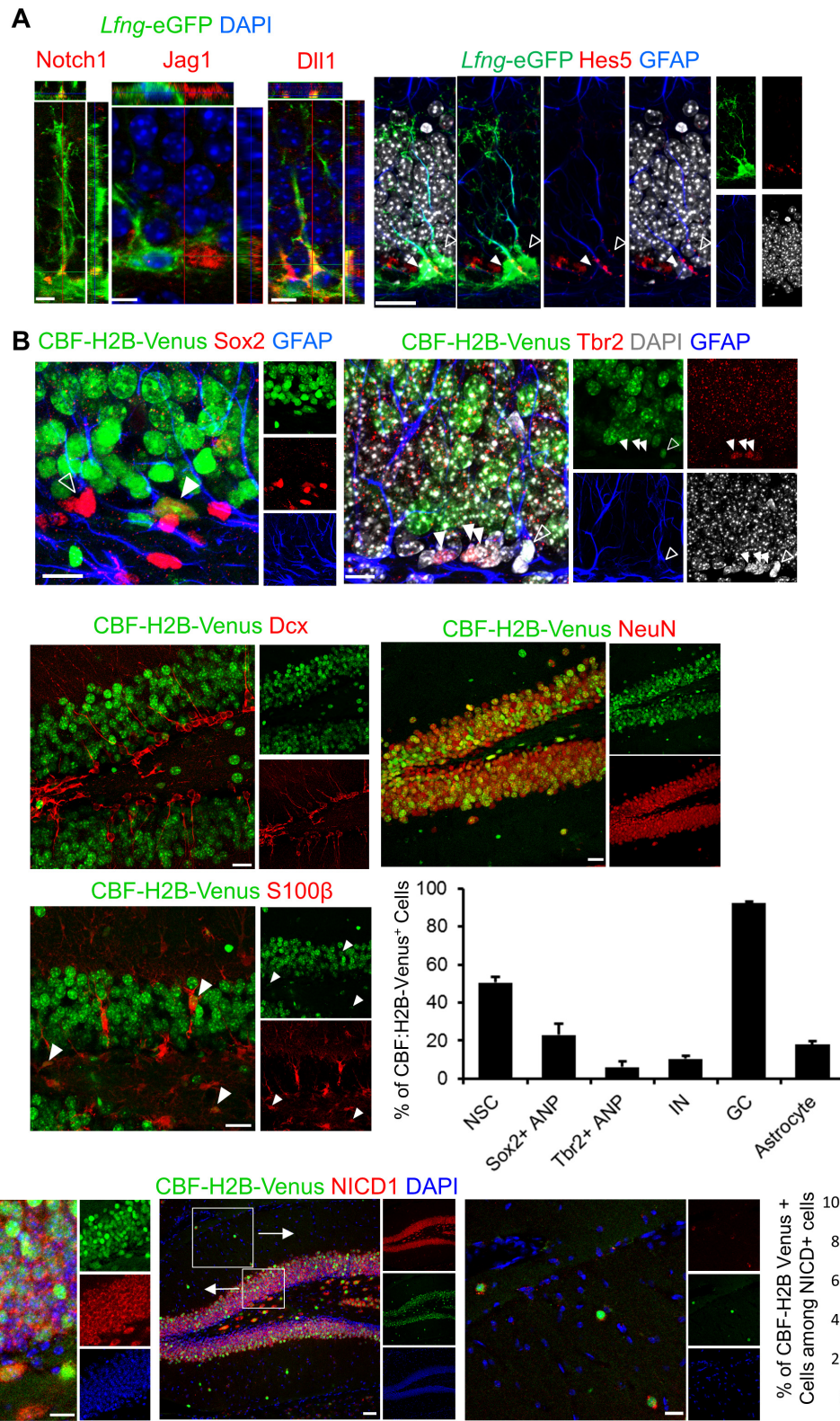


Figure 4. Notch pathway elements are present in the SGZ NSC niche. (A) Notch1 is expressed in *Lfng*-eGFP NSCs, facing granule cell layer, where late ANPs (type 2b cells) and granule cells are located. Jag1 is expressed in adjacent ANP, and Dll1 on adjacent granule cell-NSC boundary. Hes5, Figure 4 continued on next page

Figure 4 continued

downstream target of canonical Notch signaling pathway, is present in some (arrowhead) but not all (empty arrowhead) NSCs. *Scale bar* = 10 μm (Notch1, Jag1, Dll1); 20 μm (Hes5). (B) Venus is expressed in some (arrowhead) but not all (empty arrowhead) NSCs (Sox2+ cell body and GFAP+ process) in CBF:H2B-Venus mice. Type 2b cells (Tbr2) and most of the neuroblasts and immature neurons are Venus -, whereas almost all granule cells (NeuN+) are Venus+ with various degrees of intensity. Some of the mature astrocytes (S100 β +) have active Notch signaling (arrowheads). Quantification of Venus signal among various cell types reveals that most of the differentiating cells are devoid of active Notch signaling. As soon as the neurogenic differentiation finishes, Notch signaling is turned on again in the granule cells. *Scale bar* = 10 μm upper panels and 20 μm middle and lower panels. (C) NICD1 and Venus colocalize in CBF:H2B-Venus mice. NICD1 almost completely overlaps with the Venus signal in the SGZ (left inset), while it is lacking in the molecular layer (right inset). *Scale bar* = 20 μm . Quantification of Venus+ cells among NICD1+ cells in GZ and SGZ verifies high degree of colocalization (N = 3; $90.79 \pm 0.77\%$ and $96.95 \pm 0.57\%$, respectively).

DOI: [10.7554/eLife.24660.008](https://doi.org/10.7554/eLife.24660.008)

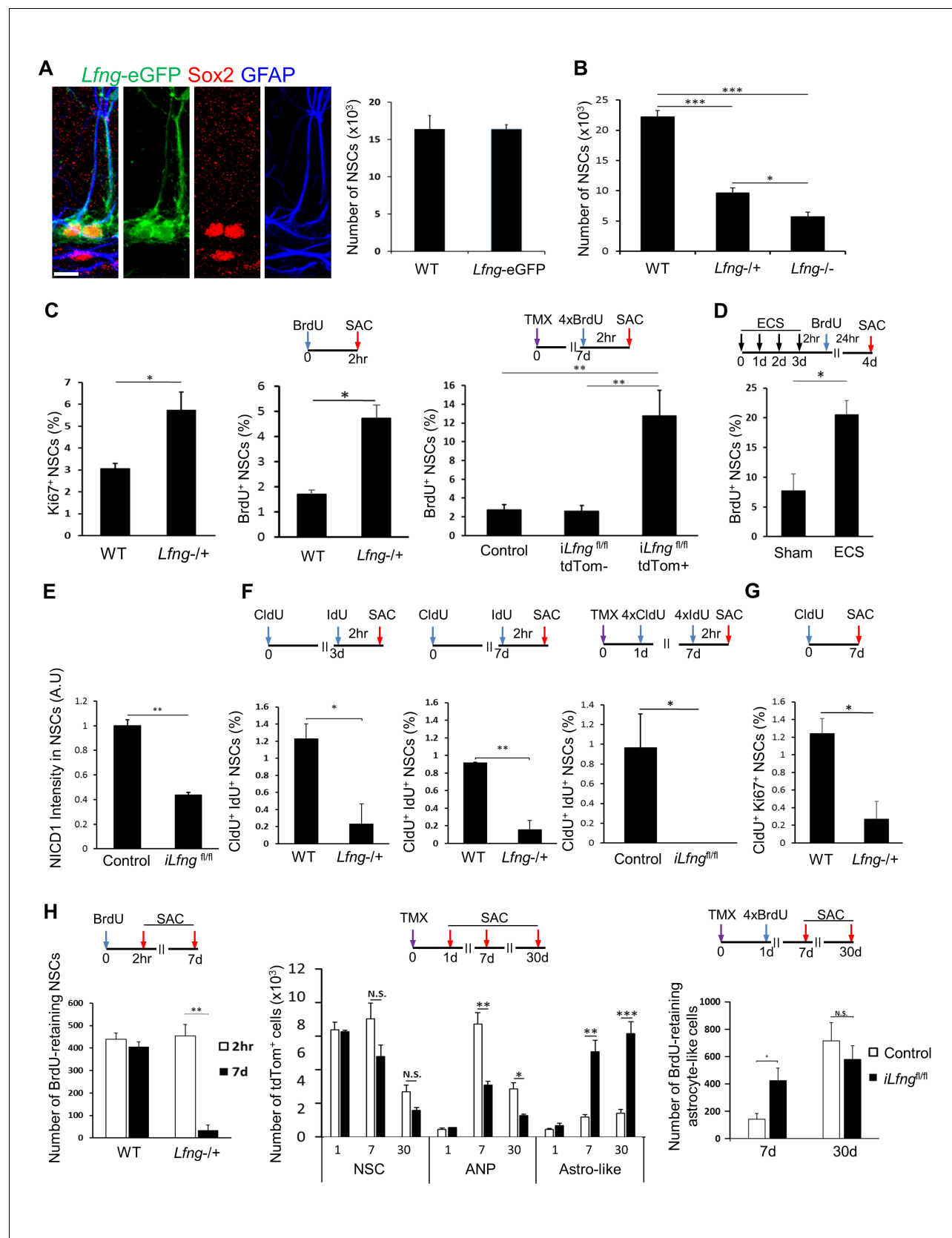


Figure 5. *Lfng* preserves NSCs by controlling their cell cycle. (A) Left panel: *Lfng*-eGFP NSCs express GFAP⁺ radial processes originating from the Sox2⁺ cell nuclei located in the SGZ. Right panel: The total number of GFAP⁺ Sox2⁺ NSCs in 4-month-old wild-type mice does not differ from the total

Figure 5 continued on next page

Figure 5 continued

number of eGFP⁺ NSCs in 4 month-old *Lfng*-eGFP (N = 3 per group; Student's t-test, p=0.99). Scale bar = 10 μ m. (B) The total number of NSCs in 2-month-old wild-type, *Lfng* heterozygote (*Lfng*^{-/+}), and homozygote (*Lfng*^{-/-}) knockout mice shows *Lfng* dose-dependent decrease in the NSC population (N = 3–4 per group; One-way ANOVA p<0.00001, Tukey HSD post-hoc test: p<0.0001 for wild-type vs *Lfng*^{-/+} or *Lfng*^{-/-}, p=0.0484 for *Lfng*^{-/+} vs *Lfng*^{-/-}). (C) Lack of *Lfng* promotes increased division of NSCs. *Left panel*: NSCs lacking *Lfng* have a higher ratio of cycling Ki67⁺ NSCs compared to wild-type (N = 4 per group; Student's t-test p=0.0221). *Middle panel*: NSCs lacking *Lfng* have a higher ratio of actively dividing, BrdU⁺ NSCs compared to wild-type (N = 4 per group; Student's t-test p=0.0017). *Right panel*: *Lfng* acts cell-autonomously and in a dose-dependent manner to control the NSC division (N = 4 per group). The ratio of BrdU⁺ NSCs was compared between *iLfng*^{fl/fl} mutant clones (tdTomato⁺), *iLfng*^{fl/fl} wild type clones (tdTomato⁻ GFAP⁺ Sox2⁺), and *Lfng*-CreER²; RCL-tdT control mice (tdTomato⁺ GFAP⁺ Sox2⁺). N = 4; p=0.9978 for control vs *iLfng*^{fl/fl} tdTomato⁻ clones; p=0.0049 for control vs *iLfng*^{fl/fl} tdTomato⁺ clones; p=0.0045 for *iLfng*^{fl/fl} tdTomato⁻ clones vs *iLfng*^{fl/fl} tdTomato⁺ clones. (D) NSCs lacking *Lfng* are hyper-activated in response to ECS treatment (N = 3–4 per group; Student's t-test, p=0.0178). (E) Lack of *Lfng* decreases Notch signal intensity in mutant NSCs. Relative intensities of NICD1 staining are significantly lower in *iLfng*^{fl/fl} mutant NSCs compared to control (N = 4 for control; N = 3 for *iLfng*^{fl/fl}; Student's t-test, p=0.0004). (F) NSCs lacking *Lfng* spend less time in the active state than wild-type NSCs. *Lfng* absence is associated with decreased S-phase re-entry 3 (*left panel*) and 7 (*middle panel*) days following the initial division compared to the wild-type NSCs (N = 4 per group; Student's t-test, p=0.0024 for 3d, p=0.0003 for 7d). CldU⁺ IdU⁺ cells represent NSCs that underwent first division at the time of CldU injection (day 0) and were in S-phase at the time of IdU injection (day 3 or day 7). *Right panel*: In *iLfng*^{fl/fl} mice, no NSCs were found that re-entered S-phase 7 days after the initial division. CldU⁺ IdU⁺ cells represent NSCs that were induced at day 0, underwent first division 1 day post-induction (CldU⁺) and were in S-phase 7 days post-induction (IdU⁺; N = 3–4 per group; Student's t-test, p=0.0014). (G) NSCs lacking *Lfng* mostly exit cell cycle within a week of first division. CldU⁺ Ki67⁺ NSCs represent NSCs that are actively cycling 7 days following the CldU injection (N = 4; Student's t-test, p=0.0105). (H) NSCs lacking *Lfng* give rise to astrocyte-like cells. *Left panel*: The number of BrdU-retaining NSCs 7 days after the BrdU injection is significantly reduced in *Lfng*^{-/+} mice compared to wild-type (N = 4 per timepoint; Student's t-test, p=0.0003). *Middle panel*: In *iLfng*^{fl/fl} mice, significantly more tdTomato⁺ astrocyte-like cells accumulate 7 and 30 days following induction compared to controls, while the number of tdTomato⁺ ANPs significantly decreases (N = 4 per group, p=0.0003 and p<0.0001 for astrocyte-like cells, p=0.0024 and p=0.0049 for ANPs). *Right panel*: The number of BrdU-retaining astrocyte-like cells 7 days after the BrdU injection is significantly higher in *iLfng*^{fl/fl} mice compared to controls, but the difference is lost at 30 days (N = 4 per group; Student's t-test, p=0.0302 for 7 days, p=0.4412 for 30 days). Bars represent mean \pm SEM. *p<0.05, **p<0.001, ***p<0.0001. See **Figure 5—figure supplement 1** for further details.

DOI: 10.7554/eLife.24660.009

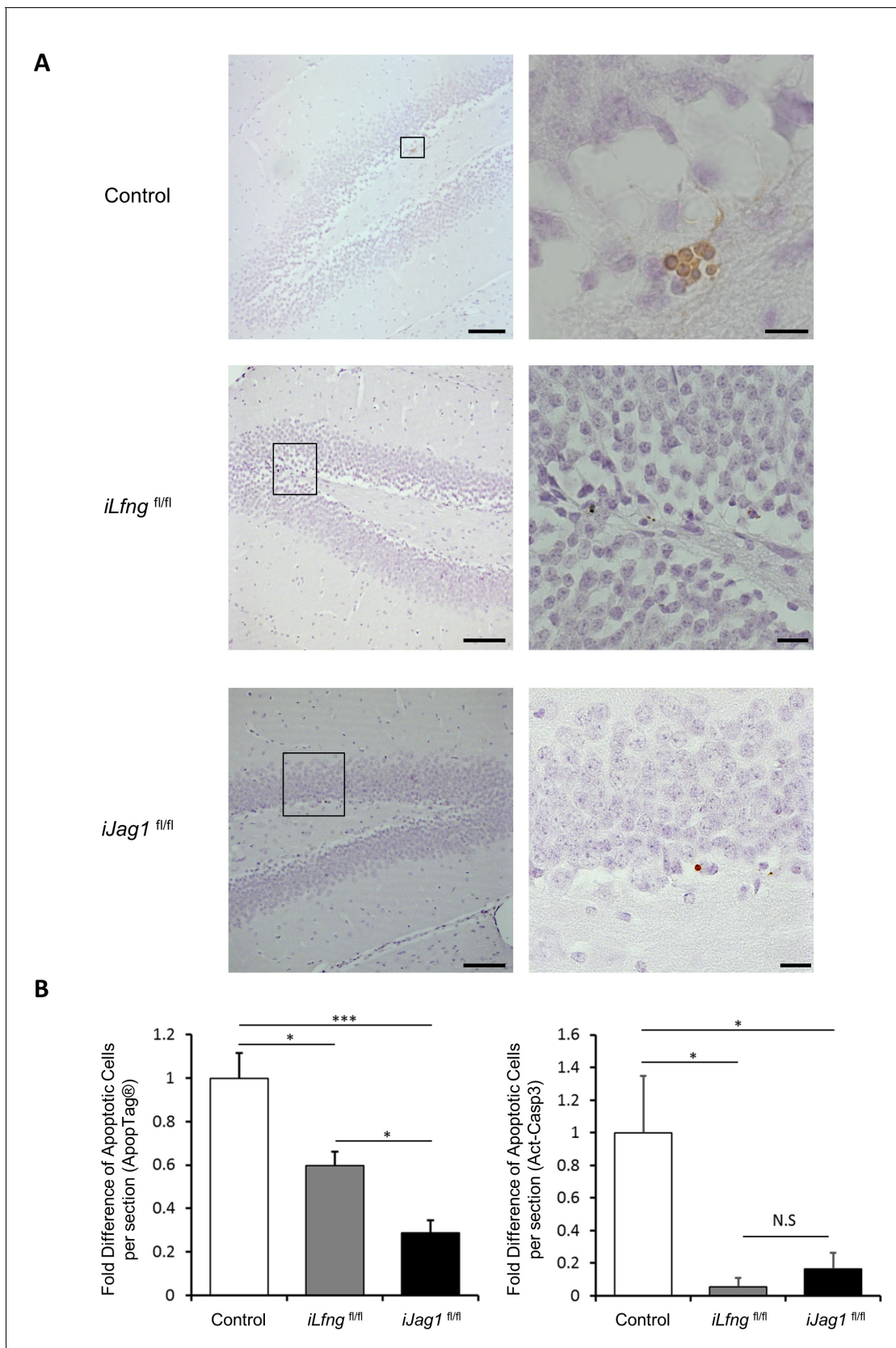


Figure 5—figure supplement 1. *Jag1* and *Lfn* affect cell survival in the SGZ. (A) ApopTag immunostaining in control, *iLfn^{fl/fl}*, and *iJag1^{fl/fl}* mice. Regions outlined in left images are presented in high magnification on the right. Scale bars = 100 μ m (low magnification); 20 μ m (high magnification). Figure 5—figure supplement 1 continued on next page

Figure 5—figure supplement 1 continued

(B) Cell death is significantly decreased in $iLfn\text{g}^{fl/fl}$ and $iJag1^{fl/fl}$ SGZ in comparison to control both by ApopTag-based (left) and activated caspase 3 (act-casp3)-based (right) detection methods. The average number of ApopTag or act-casp3+ cells in control mice was used for normalization (N = 3 per group; One-way ANOVA $p < 0.00001$, Tukey HSD post-hoc test: i) ApopTag: $p = 0.006$ for control vs $iLfn\text{g}^{fl/fl}$, $p = 0.0375$ for $iLfn\text{g}^{fl/fl}$ vs $iJag1^{fl/fl}$, $p < 0.00001$ for control vs $iJag1^{fl/fl}$; ii) act-casp3: $p = 0.0089$ for control vs $iLfn\text{g}^{fl/fl}$, $p = 0.9261$ for $iLfn\text{g}^{fl/fl}$ vs $iJag1^{fl/fl}$, $p = 0.0224$ for control vs $iJag1^{fl/fl}$). Bars represent mean \pm SEM. * $p < 0.05$, ** $p < 0.001$.

DOI: [10.7554/eLife.24660.010](https://doi.org/10.7554/eLife.24660.010)

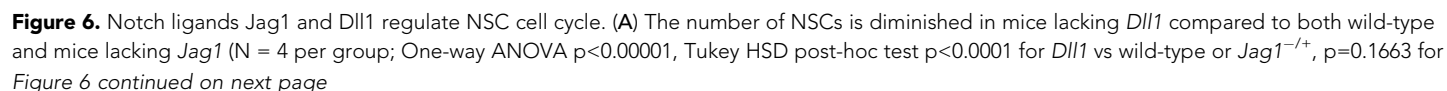


Figure 6 continued

wild-type vs $Jag1^{-/+}$. (B) Lack of either *Dll1* or *Jag1* promotes increased division of NSCs. *Left panel*: Absence of *Dll1* or *Jag1* is associated with significantly higher proportion of cycling, Ki67⁺ NSCs (N = 4 per group; One-way ANOVA $p < 0.00001$, Tukey HSD post-hoc test $p < 0.0001$ for wild-type vs $Dll1^{-/+}$ or $Jag1^{-/+}$, $p = 0.046$ for $Dll1^{-/+}$ vs $Jag1^{-/+}$). *Middle panel*: Mice lacking *Dll1* have significantly higher proportion of dividing, BrdU⁺ NSCs compared to both wild-type and $Jag1^{-/+}$ mice (N = 4 per group; One-way ANOVA $p < 0.0005$, Tukey HSD post-hoc test $p = 0.0007$ for wild-type vs $Dll1^{-/+}$, $p = 0.0015$ for $Jag1^{-/+}$ vs $Dll1^{-/+}$, $p = 0.8393$ for wild-type vs $Jag1^{-/+}$). *Right panel*: Absence of both copies of *Jag1* in $iJag1^{fl/fl}$ mice is associated with significantly higher proportion of actively dividing, BrdU⁺ NSCs compared to controls (N = 4 per group; Student's t-test, $p = 0.0028$). (C) Lack of *Dll1* has an opposite effect on NSC S-phase re-entry compared to lack of *Jag1*. Relative number of NSCs that re-enter S-phase 3 (*left panel*) and 7 (*middle panel*) days following the initial division is significantly lower in mice lacking *Dll1* at 7 days, while it is significantly higher at both timepoints in mice lacking *Jag1* compared to wild-type mice (for 3d: N = 4 per group; One-way ANOVA $p = 0.0074$, Tukey HSD post-hoc test $p = 0.9624$ for wild-type vs $Dll1^{-/+}$, $p = 0.011$ for $Jag1^{-/+}$ vs $Dll1^{-/+}$, $p = 0.0164$ for wild-type vs $Jag1^{-/+}$; for 7d: N = 4 per group; One-way ANOVA $p < 0.0001$, Tukey HSD post-hoc test $p = 0.0016$ for wild-type vs $Dll1^{-/+}$, $p < 0.0001$ for $Jag1^{-/+}$ vs $Dll1^{-/+}$, $p = 0.0002$ for wild-type vs $Jag1^{-/+}$). CldU⁺ IdU⁺ cells represent NSCs that underwent first division at the time of CldU injection (day 0) and were in S-phase at the time of IdU injection (day 3 or day 7). *Right panel*: In $iJag1^{fl/fl}$ mice, significantly higher proportion of NSCs re-enter S-phase 6 days following the initial division compared to controls (N = 4 per group; Student's t-test, $p = 0.0003$). CldU⁺ IdU⁺ cells represent NSCs that were induced at day 0, underwent first division at 1 day post-induction (CldU⁺) and were in S-phase (IdU⁺) at 7 days post-induction. (D) Lack of *Dll1* has an opposite effect on NSC cycling time compared to lack of *Jag1* (N = 4 per group; One-way ANOVA $p < 0.00001$, Tukey HSD post-hoc test $p = 0.0049$ for wild-type vs $Dll1^{-/+}$, $p = 0.005$ for wild-type vs $Jag1^{-/+}$ and $p < 0.0001$ for $Dll1^{-/+}$ vs $Jag1^{-/+}$). CldU⁺ Ki67⁺ NSCs represent NSCs that are cycling 7 days following the CldU injection. (E) Lack of *Jag1* increases Notch signal intensity in NSCs. Relative intensities of NICD1 staining are significantly higher in *Jag1* mutant NSC clones compared to control NSCs (N = 3 for $iJag1^{fl/fl}$, N = 4 for control; Student's t-test $p < 0.0255$). (F) In $Dll1^{-/+}$ mice, no NSCs that retained BrdU 7 days after the BrdU injection were detected. In $Jag1^{-/+}$ mice, the absolute number of BrdU-retaining NSCs is significantly higher at both timepoints compared to wild-type mice, suggesting increased self-renewal of NSCs lacking *Jag1* (For 7d: N = 4 per group; One-way ANOVA $p < 0.00001$, Tukey HSD post-hoc test $p < 0.0001$ for wild-type vs $Jag1^{-/+}$ and $Jag1^{-/+}$ vs $Dll1^{-/+}$, and $p = 0.0035$ for wild-type vs $Dll1^{-/+}$. For 2hr-7d comparisons: $p = 0.0028$ for $Jag1^{-/+}$ and $p = 0.001$ for $Dll1^{-/+}$ mice). (G) *Left graph*: Mice lacking *Jag1* have significantly more Sox2⁺ ANPs compared to both wild-type and mice lacking *Dll1* (N = 4; One-way ANOVA $p < 0.00001$; $p < 0.00001$ for wild-type vs $Jag1^{-/+}$ and $Dll1^{-/+}$ vs $Jag1^{-/+}$; $p = 0.2828$ for wild-type vs $Dll1^{-/+}$). *Right graph*: Average size of Ki67⁺ clusters around Ki67⁺ NSCs is larger in $Jag1^{-/+}$ mice compared to wild-type and $Dll1^{-/+}$ mice (N = 4; One-way ANOVA $p < 0.00001$; $p = 0.0001$ for wild-type vs $Jag1^{-/+}$; $p = 0.0015$ for wild-type vs $Dll1^{-/+}$, $p < 0.0001$ for $Dll1^{-/+}$ vs $Jag1^{-/+}$). (H) One month following BrdU injection, $Dll1^{-/+}$ mice have significantly higher ratio of S100 β ⁺ progeny among newly generated cells compared to wild-type (N = 4; Student's t-test, $p = 0.016$). (I) In $iJag1^{fl/fl}$ mice, significantly more tdTomato⁺ NSCs accumulate at 7 and 30 days post-induction compared to controls, suggesting increased self-renewal in *Jag1* mutant NSCs. This is accompanied by increased number of tdTomato⁺ ANPs (N = 4 per group; $p = 0.0263$ and $p < 0.0001$ for NSCs at 7d and 30d, respectively; $p = 0.0033$ and $p = 0.069$ for ANPs at 7d and 30d, respectively). Please note that all wild-type and control mice presented here are same as in **Figure 5**, as the experiments using the knockout lines ($Lfng^{-/+}$, $Dll1^{-/+}$, $Jag1^{-/+}$, $iLfng^{fl/fl}$, $iJag1^{fl/fl}$) were done at the same time. The results are presented in two figures for clarity. Bars represent mean \pm SEM* $p < 0.05$, ** $p < 0.001$, *** $p < 0.0001$. See **Figure 6—figure supplement 1** for further details.

DOI: 10.7554/eLife.24660.011

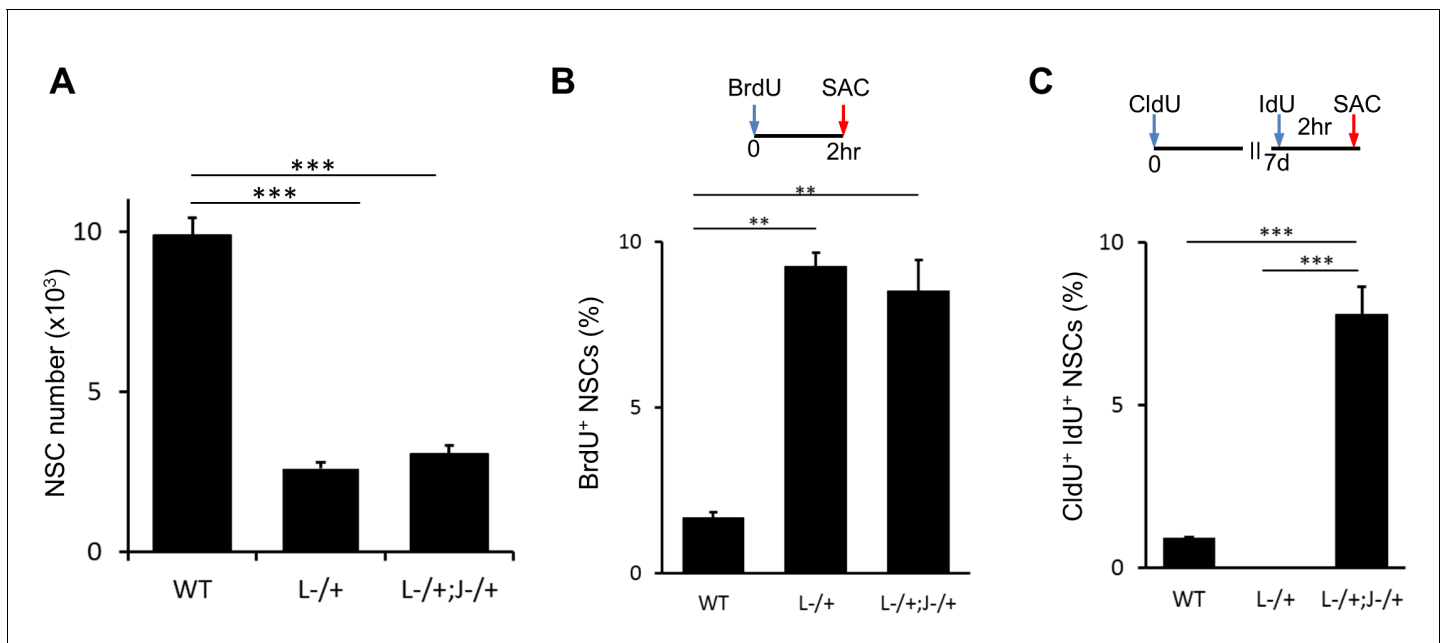


Figure 6—figure supplement 1. Lack of both *Lfng*^{-/+} and *Jag1*^{-/+} has additive effect on NSCs. (A) The number of NSCs in 6 month old *Lfng*^{-/+} (L-/+) and *Lfng*^{-/+}; *Jag1*^{-/+} (L-/+;J-/+) mice is significantly lower compared to wild-type mice (N = 3 for *Lfng*^{-/+} and *Lfng*^{-/+}; *Jag1*^{-/+} and N = 4 wild-type; One-way ANOVA p<0.00001, Tukey HSD post-hoc test: p<0.0001 for wild-type vs *Lfng*^{-/+} and *Lfng*^{-/+}; *Jag1*^{-/+}; and p=0.6869 for *Lfng*^{-/+} vs *Lfng*^{-/+}; *Jag1*^{-/+}). (B) As in *Lfng*^{-/+} mice, NSCs in *Lfng*^{-/+}; *Jag1*^{-/+} mice have higher ratio of actively dividing BrdU⁺ NSCs compared to wild-type mice (N = 3; One-way ANOVA p<0.0002, Tukey HSD post-hoc test: p=0.0001 for wild-type vs *Lfng*^{-/+}, p=0.0003 for wild-type vs *Lfng*^{-/+}; *Jag1*^{-/+}, p=0.6724 for *Lfng*^{-/+} vs *Lfng*^{-/+}; *Jag1*^{-/+}). (C) *Lfng*^{-/+}; *Jag1*^{-/+} double knockout mice have significantly higher proportion of NSCs re-entering S-phase 1 week following the initial division compared to wild-type (N = 3; One-way ANOVA p<0.0001, Tukey HSD post-hoc test: p<0.00001 for wild-type vs *Lfng*^{-/+}; *Jag1*^{-/+} and *Lfng*^{-/+} vs *Lfng*^{-/+}; *Jag1*^{-/+}). Bars represent mean ± SEM. **p<0.001, ***p<0.0001.

DOI: 10.7554/eLife.24660.012

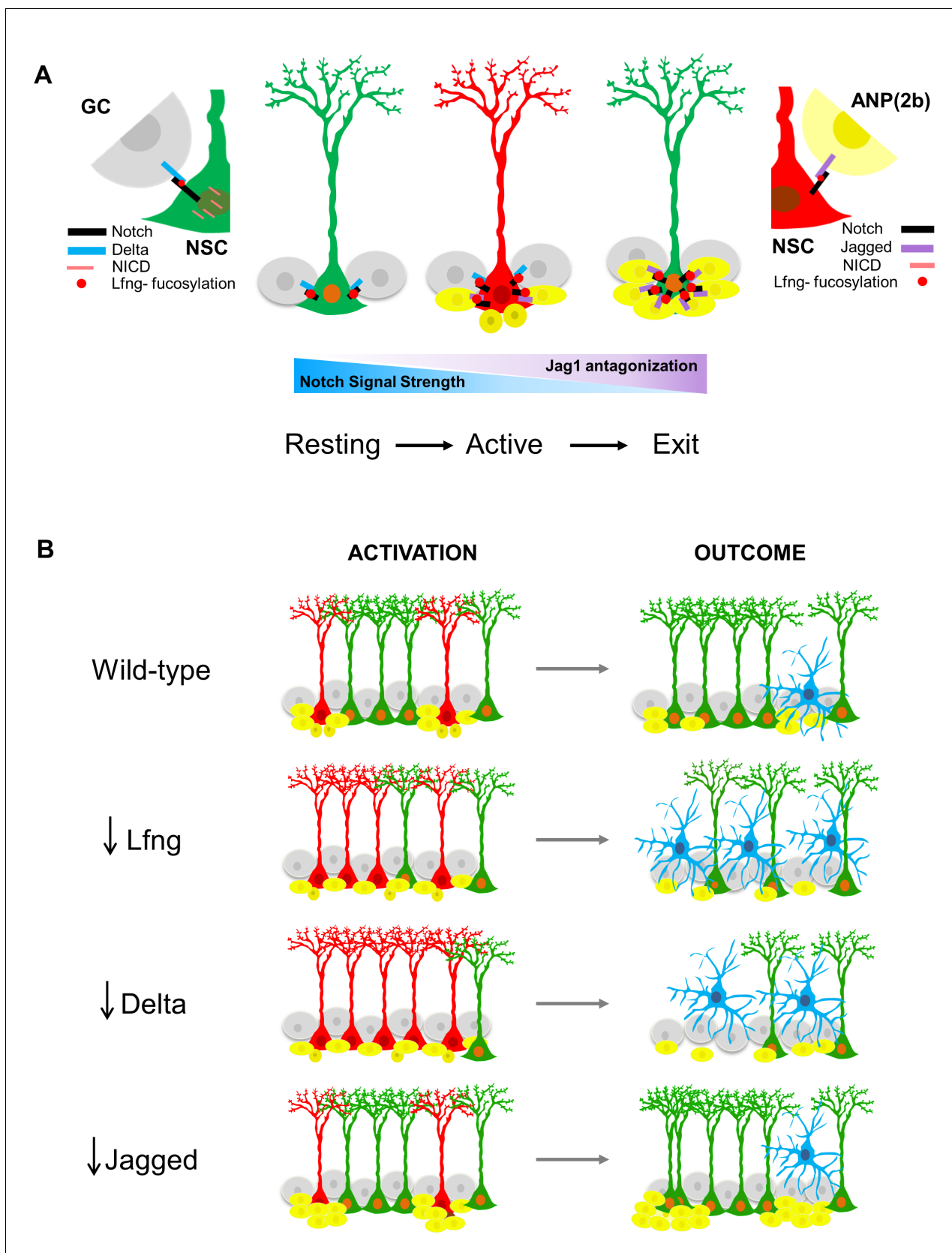


Figure 7. Proposed model for Lfng-mediated regulation of NSC maintenance by progeny. (A) In the resting state, Lfng-expressing NSC (green) is surrounded mostly by Delta1 (Dll)-expressing granule cells (GC, grey). Dll1 binds to the Lfng-modified Notch receptor on the NSC, which boosts Dll1-
 Figure 7 continued on next page

Figure 7 continued

mediated Notch signaling by producing more NICDs and the NSC is kept quiescent but ready to undergo cell cycle if stimulated. Once activated, NSC (red) starts to produce ANPs. The first progeny (Type 2a, small dark yellow cells) do not express Notch ligands and the NSC continues to divide. As ANPs mature into late ANPs (Type 2b, yellow cells), they start to express Jag1. Jag1 binding to the Lfng-modified Notch receptor on the NSC does not generate NICD and thus the Notch signaling strength in the 'mother' NSC decreases. Eventually, the NSC is surrounded by mostly Jag1-expressing ANPs, and it exits active state (green NSC). Thus, in the resting state, the granule cell progeny prevents overt activation of NSCs, while in the active state, the ANP progeny prevents overt division of the NSC. These feedback signaling from the progeny both act to preserve the NSC population and the integrity of the niche. (B) The summary of the loss-of-function data, focusing on the number of activated NSCs (red) and the final outcomes of their division. Mice lacking *Lfng* and *Dll1* have similar phenotypes: NSCs are recruited in bulk, they divide less and faster, and eventually lead to depletion of NSC population. In *Lfng* mutant mice, there is an increased transformation into astrocytes (blue). Mice lacking *Jag1* have the opposite phenotype: while NSCs are activated as in the wild-type, they divide more and longer, and produce large clusters of ANPs as well as self-renew.

DOI: [10.7554/eLife.24660.013](https://doi.org/10.7554/eLife.24660.013)